Bulletin of the Seismological Society of America, Vol. 102, No. 2, pp. 812–821, April 2012, doi: 10.1785/0120110141

Modeling Repeated Slip Failures on Faults Governed by Slip-Weakening Friction

by Andrea Bizzarri

Abstract The single-body mass-spring analog model has been largely used to simulate the recurrence of earthquakes on faults described by rate- and state-dependent rheology. In this paper, the fault was assumed to be governed by the classical slip-weakening (SW) law in which the frictional resistance linearly decreases as the developed slip increases. First, a closed-form fully analytical solution to the 1D elastodynamic problem was derived, expressing the time evolution of the slip and its time derivative. Second, a suitable mechanism for the recovery of stress during the interseismic stage of the rupture was proposed, and this stress recovery was shown quantitatively to make possible the simulation of repeated instabilities with the SW law. Moreover, the theoretical predictions were shown to be compatible with the numerical solutions obtained by adopting a rate and state constitutive model. The analytical solution developed here is, by definition, dynamically consistent and nonsingular. Moreover, the slip velocity function within the coseismic time window found here can be easily incorporated into slip inversion algorithms.

Scientific Rationale

There are two concepts that have been strongly emphasized in the mechanics of earthquake faulting: (1) it is not possible to obtain a closed-form analytical solution to the spontaneous dynamic rupture problem (i.e., without a prior imposed rupture velocity) for an extended fault (2D or 3D problems), and (2) there is no consensus on the expression of the fault friction (i.e., on the governing law that describes the various phenomena occurring during an earthquake instability; Bizzarri, 2009).

As discussed in Bizzarri (2011b), many different friction models have been proposed in the literature. The most largely employed models are the slip-dependent laws, where the frictional resistance is a function of the displacement discontinuity (slip) across the sliding interface, and the more elaborate nonlinear rate- and state-dependent (RS) friction laws, which are mainly dependent on the slip velocity and on some state variables, thereby accounting for the memory of the previous slip episodes (Ruina, 1983; Marone, 1998 and references cited therein).

Studies of dynamic models of extended, fully dynamic, and spontaneous ruptures showed that the classical (i.e., linear) slip-weakening (SW) equation (Ida, 1972) is able to reproduce all of the main features of a single instability event, as rate and state laws do (Okubo, 1989; Cocco and Bizzarri, 2002): the stress release and the consequent excitation of seismic waves in the medium surrounding the fault, a finite energy flux at the crack tip, and the breakdown processes occurring over a finite distance. In addition, the numerical implementation of the SW model is straightforward, and this law has the fundamental advantage of allowing the modeler to clearly define and assign *a priori* (i.e., as input parameters) all of the levels of stress and the scale distance over which the stress release is accomplished (and thus of the so-called fracture energy, required for the rupture to advance; Bizzarri, 2010b).

The most severe physical limitation attributed to the classical SW model is that, contrary to the RS laws (Gu *et al.*, 1984; Bizzarri, 2010c, among many others), in its canonical formulation it is not able to reproduce further instabilities on the same seismogenic structure; that is, it is unable to simulate the stress recovery during the interseismic period that leads to subsequent slip failures. This is the reason why the classical SW model has never been implemented in mass-block models of faults. Aochi and Matsu'ura (2002) presented numerical solutions to a spring-slider model by adopting a more complicated friction law, in particular, a nonlinear slip-dependent constitutive equation with an additional explicit dependence on the time, which accounts for adhesion and abrasion effects.

The main objectives of the present study were twofold: (1) to find an analytical solution to the dynamic problem in the case of a single-body (1D) mass-spring analog fault model and (2) to propose a suitable modification to the SW law that would lead to the interseismic stress recovery. Therefore, I show that it is possible to simulate the whole seismic cycle with repeated earthquake ruptures on the same

fault even in the framework of the simple SW friction governing model, which is in general agreement with the results from the RS friction law.

The Adopted Constitutive Model

In the present paper, the frictional resistance τ was assumed to be a linear function of the slip $\bar{u}$ developed during an instability:

$$\tau = \begin{cases} \left[\mu_u - (\mu_u - \mu_f)\frac{\bar{u}}{d_0}\right]\sigma_n^{\text{eff}}, & \bar{u} < d_0 \\ \mu_f \sigma_n^{\text{eff}} + f(\bar{t}), & \bar{u} \geq d_0, \tau < \tau_u \end{cases}, \quad (1)$$

where μ_u and μ_f define the yield and the residual levels of stress, respectively ($\tau_u = \mu_u \sigma_n^{\text{eff}}$ and $\tau_f = \mu_f \sigma_n^{\text{eff}}$), d_0 is the characteristic SW distance over which τ decreases ($\tau = \tau_f$ when $\bar{u} = d_0$), σ_n^{eff} is the effective normal stress (which can account for possible temporal variations due to the thermal pressurization of pore fluids; Bizzarri and Cocco, 2006), and $f(\bar{t})$ is a function of the time $\bar{t}$ elapsed after the completion of the stress release that occurs during an instability event. The function f represents the assumed time history of the stress during the interseismic period in a sequence of stick–slip events. In this paper, the following was assumed:

$$f(\bar{t}) = Rkv_{\text{load}}\bar{t}, \quad (2)$$

where R is a dimensionless tuning parameter controlling the stress recovery and $kv_{\text{load}} = \dot{\tau}_{\text{load}}$ is the loading rate of tectonic origin. The function $f(\bar{t})$ is responsible for the stress recovery because it causes an increase in τ up to τ_u; at this instant, another instability occurs. (Recall here that, in the SW framework, a dynamic instability is realized when τ first reaches τ_u.) As will be discussed in the remainder of the paper, the recurrence interval is not simulated by the model, as in the case of the RS laws (Rice and Tse, 1986), but it is imposed through the choice of $f(\bar{t})$. In light of this knowledge, the physical interpretation of the parameter R is the following: a zero value for R gives zero stress recovery so that the stress on the fault never reaches the yield strength and no subsequent seismic events occur, meaning that all deformation is accommodated by slow aseismic creep either on the fault or on some subsidiary structure occurring at a rate equal to the plate velocity. If R is 1, all tectonic loading is accommodated by seismicity on the fault, and when R is between 0 and 1, some creep is occurring, in effect lengthening the cycle time of the seismic events.

Interestingly, within the coseismic time window (pertaining to the stress release process and having a duration of tens of seconds), the function $f(\bar{t})$ is negligible with respect to τ_f, and therefore the governing model described in equation (1) reduces to the canonical formulation of Ida (1972), in which τ remains equal to τ_f. Note that $f(\bar{t})$ becomes important in the interseismic stage of the rupture.

Fully Analytical Solution to the 1D Elastodynamic Equation

The spring-slider model with one degree of freedom, which has been largely employed to describe the whole history of a seismogenic fault (Rice and Tse, 1986, among others), was used here. For this analog fault system, the equation of motion is that of a harmonic oscillator:

$$m\ddot{u} = kv_{\text{load}}t - ku - \tau - c\dot{u}, \quad (3)$$

where the overdots indicate the time derivatives, m is the mass equivalent of the fault (per unit surface; $m = k[T/(2\pi)]^2$, where T is the vibration period of the frictionless oscillator), k is the elastic constant of the spring (accounting for the elastic medium cut by the fault interface), and v_{load} is the imposed loading velocity at the end of the spring (physically interpreted as the speed of a tectonic plate loading the seismogenic region under study). The fault stiffness can be associated with the static stress drop and the total slip developed during the failure event (Walsh, 1971). The load applied to the system, $kv_{\text{load}}t$, gives the tectonic loading rate $\dot{\tau}_{\text{load}} = kv_{\text{load}}$ appearing in equation (2). The last term in equation (3), where the constant c depends on the parameters of the medium in which the fault is embedded, expresses the so-called radiation damping (Rice, 1993), introduced to simulate the energy lost as propagating seismic waves. In equation (3), which of course is a proxy of the true behavior of an extended fault embedded in a continuous medium, τ represents the frictional resistance; in particular, τ is assumed to follow equation (1).

For a graphical illustration of this model, see figure S1 of the auxiliary material in Bizzarri (2010c).

First Weakening Episode

As is well known, within the SW framework, the fault is locked until the frictional resistance reaches the upper yield stress τ_u. This occurs at the time $t_{\text{first}} = \tau_u/(kv_0)$, which corresponds to the onset time of the first instability (v_0 is the initial velocity of the loading point), and therefore $u(t') = 0$, $\forall\ t' \leq t_{\text{first}}$. For the sake of simplicity, in the remainder of the paper, the time elapsed since t_{first} is denoted by the symbol t (t_{first} is the origin of times). Let us also assume that $v_0 = v_{\text{load}}$.

By construction, at $t = 0$, the loading point displacement is $u_{\text{load}} = \tau_u/k$, $v(0) = v_0$, and $\tau(0) = \tau_u$; after the slider moves (i.e., for $t > 0$), the frictional resistance is described by equation (1), with $\bar{u} = u$ because $u(0) = 0$. It was also observed that, during a coseismic instability, u_{load} can be considered to be constant and the function $f(\bar{t})$ can be neglected so that the constitutive model (1) reduces to the classical SW law, as discussed in The Adopted Constitutive Model section. Consequently, the solutions to equation (3) are

$$u(t) = \frac{mv_0}{C_2}\left\{\exp\left[-\frac{(c-C_2)t}{2m}\right] - \exp\left[-\frac{(c+C_2)t}{2m}\right]\right\} \tag{4}$$

and

$$v(t) = \frac{v_0}{2C_2}\left\{-(c-C_2)\exp\left[-\frac{(c-C_2)t}{2m}\right] + (c+C_2)\exp\left[-\frac{(c+C_2)t}{2m}\right]\right\}, \tag{5}$$

where the following quantities, constant through time, have been introduced:

$$\Delta\tau_b \equiv \tau_u - \tau_f, \qquad C_1 \equiv d_0 k - \Delta\tau_b,$$
$$\text{and} \quad C_2 \equiv \sqrt{\frac{c^2 d_0 - 4mC_1}{d_0}}. \tag{6}$$

Note that equations (4) and (5) are real-valued functions when the following condition holds:

$$C_1 \le \frac{c^2 d_0}{4m} \quad \text{or equivalently} \quad \Delta\tau_b \ge \frac{d_0}{4m}(4km - c^2). \tag{7}$$

The previous solutions (4) and (5) hold up in the instant when u first reaches d_0; let this instant be denoted by the symbol t_f (in particular, $t_f = T_b$, where T_b is the breakdown time, expressing the time required for τ to complete the breakdown stress drop $\Delta\tau_b = \tau_u - \tau_f$; Bizzarri *et al.*, 2001). Now $u_f \equiv u(t_f) = d_0$ by definition and $v_f \equiv v(t_f)$, which is known from equation (5). Also in this case, for a time window that is small with respect to the interseismic stress recovery process, $u_{\text{load}} = \tau_u/k$ and $\tau = \tau_f$. For typical values of the parameters (see Table 1), $c^2 - 4km < 0$; therefore, a solution to the elastodynamic problem is sought in the form $g(\tilde{t}) + \exp(-\frac{c\tilde{t}}{2m})[c_1\cos(\omega\tilde{t}) + c_1\sin(\omega\tilde{t})]$, where g is a function of $\tilde{t}$ and

$$\tilde{t} \equiv t - t_f, \qquad \omega \equiv \frac{\sqrt{4km - c^2}}{2m}. \tag{8}$$

(Again, note that ω is constant through time.) By applying the initial conditions (at $t = t_f$) discussed before equation (8), g is found to be a constant ($g = \frac{\Delta\tau_b}{k}$) so that finally the following are obtained:

$$u(t) = \frac{\Delta\tau_b}{k} + \frac{\exp(-\frac{c\tilde{t}}{2m})}{2km\omega}[2C_1 m\omega\cos(\omega\tilde{t}) + (2kmv_f + cC_1)\sin(\omega\tilde{t})] \tag{9}$$

and

$$v(t) = \frac{\exp(-\frac{c\tilde{t}}{2m})}{4km^2\omega}[4km^2\omega v_f\cos(\omega\tilde{t}) - (2ckmv_f + c^2C_1 + 4C_1m^2\omega^2)\sin(\omega\tilde{t})]. \tag{10}$$

Solutions (9) and (10) hold for $t > t_f$ and therefore complement equations (4) and (5), respectively, which hold for $t < t_f$. They represent the solution within the coseismic time

Table 1
Adopted Constitutive Parameters

Parameter	Value	
	Configuration A	Configuration B
Model Parameters		
Loading velocity, v_{load}	3.17×10^{-10} m/s	3.17×10^{-10} m/s
Machine stiffness, k	10 MPa/m	10 MPa/m
Tectonic loading rate, $\dot{\tau}_0 = kv_{\text{load}}$	3.17×10^{-3} Pa/s	3.17×10^{-3} Pa/s
Period of the analog freely slipping system, $T = 2\pi\sqrt{m/k}$	5 s	5 s
Radiation damping constant, c	4.5 MPa ·s/m	4.5 MPa· s/m
Fault Constitutive Parameters		
Effective normal stress, σ_n^{eff}	30 MPa	30 MPa
Initial slip velocity, v_0	3.17×10^{-10} m/s(= v_{load})	3.17×10^{-10} m/s(= v_{load})
RS Friction Law (Equation 18) Parameters		
Logarithmic direct effect parameter, a	0.008	0.012
Evolution effect parameter, b	0.016	0.016
Characteristic scale length, L	0.01 m	0.01 m
Reference value of the friction coefficient, μ_*	0.56	0.56
Reference value of the sliding velocity, v_*	3.17×10^{-10} m/s(= v_0)	3.17×10^{-10} m/s(= v_0)
Cycle time, T_{cycle}	52.00 yr	31.40 yr
SW Model (Equation 1) Parameters		
Upper yield stress, τ_u	17.3 MPa	17.2 MPa
Kinetic friction level, τ_f	13.8 MPa	15.3 MPa
Breakdown stress drop, $\Delta\tau_b = \tau_u - \tau_f$	3.5 MPa	1.9 MPa
Characteristic SW distance, d_0	0.1 m	0.1 m
Parameter controlling the interseismic stress recovery, R	0.673	0.605

window, and they do not depend on any physical assumptions regarding the interseismic stage of the rupture.

Interseismic Phase

Equation (10) predicts that at a certain time, denoted by the symbol t_h, the slip velocity first falls to zero: $v_h \equiv v(t_h) = 0$. Correspondingly, the slip reaches its maximum value, $u_h \equiv u(t_h)$; at this instant, the slider stops. For times greater than t_h, the load pushing the slider is then expressed as $\tau_u + kv_0\bar{t}$ and the frictional resistance is now $\tau_f + R\dot{\tau}_{\text{load}}\bar{t}$, where $\bar{t} \equiv (t - t_h)$. Equation (3) can still be analytically solved with the initial conditions $u(\bar{t} = 0) = u_h$ and $v(\bar{t} = 0) = v_h = 0$. The solution exhibits a damped behavior, characterized by a time velocity that reaches the asymptotic value of $(1 - R)v_0$. This value is then maintained for the whole interseismic phase, during which τ increases according to equations (1) and (2).

Subsequent Instabilities

Because of the recovery function $f(\bar{t})$, the frictional resistance can again reach the upper value τ_u; this will occur at the time $t_u = t_f + t_{\text{rec}}$, where t_f is known from the previous instability (see the First Weakening Episode section) and t_{rec} is the recovery time. Therefore, t_{rec} can be implicitly expressed by the condition $f(t_{\text{rec}}) = \Delta\tau_b$; for the specific choice of $f(\bar{t})$ as in equation (2), t_{rec} is

$$t_{\text{rec}} = \frac{\Delta\tau_b}{Rkv_0}. \tag{11}$$

At $t = t_u$, $u_u \equiv u(t_u) = u_h + (1 - R)v_0[t_{\text{rec}} - (t_h - t_f)] \cong u_h + (1 - R)v_0 t_{\text{rec}}$, because $(t_h - t_f) \ll t_{\text{rec}}$, and $v_u \equiv v(t_u) = (1 - R)v_0$, as discussed in the section Interseismic Phase. Therefore, for times greater than t_u, the solution to equation (3) can be obtained exactly as was done previously in the sections First Weakening Episode and Interseismic Phase:

$$u(t) = u_u + \frac{m(1-R)v_0}{C_2}\left\{\exp\left[-\frac{(c-C_2)\tilde{\tilde{t}}}{2m}\right] - \exp\left[-\frac{(c+C_2)\tilde{\tilde{t}}}{2m}\right]\right\} \tag{12}$$

and

$$v(t) = \frac{(1-R)v_0}{2C_2}\left\{-(c-C_2)\exp\left[-\frac{(c-C_2)\tilde{\tilde{t}}}{2m}\right] + (c+C_2)\exp\left[-\frac{(c+C_2)\tilde{\tilde{t}}}{2m}\right]\right\}, \tag{13}$$

where

$$\tilde{\tilde{t}} \equiv t - t_u. \tag{14}$$

For slips $u - u_u \geq d_0$, following the procedure discussed in the First Weakening Episode section again yields solutions in the form of equations (9) and (10) with the actual value of v_f (now given by equation 13) and the proper shift in u, which is given by u_u. Then, after the rupture stops, a new interseismic stage is started again, where the solution is the same as that discussed in the Interseismic Phase section.

In conclusion, except for the first instability where the solution was expressed by equations (4) and (9) and their time derivatives, for all of the subsequent instabilities, the following relations hold:

$$u(t) = \begin{cases} u_u^{(n)} + \frac{m(1-R)v_0}{C_2}\left\{\exp\left[-\frac{(c-C_2)\tilde{\tilde{t}}^{(n)}}{2m}\right] - \exp\left[-\frac{(c+C_2)\tilde{\tilde{t}}^{(n)}}{2m}\right]\right\}, & u(t) - u_u^{(n)} < d_0 \\ u_u^{(n)} + \frac{\Delta\tau_b}{k} + \frac{\exp(-\frac{c\tilde{t}^{(n)}}{2m})}{2km\omega}[2C_1 m\omega\cos(\omega\tilde{t}^{(n)}) + (2kmv_f^{(n)} + cC_1)\sin(\omega\tilde{t}^{(n)})], & u(t) - u_u^{(n)} \geq d_0 \\ & t \leq t_h^{(n)} \end{cases}. \tag{15}$$

In equation (15), the superscript n denotes the values pertaining to the actual instability n ($n \geq 2$),

$$\begin{aligned} \tilde{\tilde{t}}^{(n)} &\equiv t - t_u^{(n)} = t - t_f^{(n-1)} - t_{\text{rec}}, \\ \tilde{t}^{(n)} &\equiv t - t_f^{(n)}, \\ u_u^{(n)} &\equiv u_h^{(n-1)} + (1-R)v_0 t_{\text{rec}}, \end{aligned} \tag{16}$$

and all of the other quantities have been already defined.

This iterative procedure is possible because the levels of stress are prescribed in the SW model, and therefore the recovery time (required to again reach τ_u) is always the same (see equation 11) if the variations of the effective normal stress are not considered (Bizzarri, 2010c). More interestingly, the value of v_u is the same for all of the subsequent instabilities; $v_u^{(n)} = (1 - R)v_0$, $\forall\ n \geq 2$.

This result brings to mind the concept of the stable limit cycle reached by a spring slider obeying the RS friction laws (Gu *et al.*, 1984; see also Bizzarri, 2010c). In the rate and state framework, the interevent time (i.e., the cycle time T_{cycle} modulating the permanently sustained oscillations) depends on many factors: the constitutive parameters, the analytical formulation of the governing model, and the presence

of different phenomena, such as the fluid thermal pressurization (Mitsui and Hirahara, 2009; Bizzarri, 2010c), the porosity evolution (Mitsui and Cocco, 2010; Bizzarri, 2012), and the wear processes (Bizzarri, 2010c). From equation (11), it emerges that the tuning of the parameter R makes it possible to obtain a given cycle time $T_{\rm cycle}$:

$$R = \frac{\Delta\tau_b}{kv_0 T_{\rm cycle}}. \tag{17}$$

Example of the Behavior of the System

In this section, the time evolution of the spring-slider analog fault model subject to the governing model described in equation (1) is evaluated. The solution is compared to numerical results for a system governed by the nonlinear Ruina–Dieterich (RD; Ruina, 1983) rate and state law:

$$\begin{cases} \tau = \left[\mu_* + a\ln\left(\frac{v}{v_*}\right) + \Theta\right]\sigma_n^{\rm eff} \\ \frac{\rm d}{{\rm d}t}\Theta = -\frac{v}{L}\left[\Theta + b\ln\left(\frac{v}{v_*}\right)\right] \end{cases}, \tag{18}$$

where a, b, and L are constitutive parameters, Θ is the state variable accounting for previous slip episodes, and v_* and μ_* are reference values for the sliding velocity and friction coefficient, respectively. The numerical comparison was realized as follows: First, the RD parameters were set by assuming values of a, b, and L (see Table 1) that pertain to two rather different configurations, the first one being representative of a more unstable fault (configuration A) and the second one being representative of a moderately unstable fault (configuration B). It is well known that a and b are material properties in that they depend on the pressure, temperature, and so on. This leads to significant variations in their values, also with time, and this can have significant effects on the recurrence time, as discussed elsewhere (Bizzarri, 2011a). Moreover, there is the problem of scaling the values inferred in laboratory experiments to the real-world case (Scholz, 1988). The values adopted here have been widely used in recent literature (e.g., Lapusta and Liu, 2009 and references cited therein).

Both of the selected configurations are velocity weakening (i.e., $b > a$), but in configuration A the large value of the difference $b - a$ ensures a strong velocity-weakening behavior (see equation 20). In the RD case, the problem was solved numerically as described in previous papers (e.g., Bizzarri, 2010c); the only difference was that here the radiation damping term was also included, as shown in equation (3). (This issue is discussed in more detail in the Appendix.) Then once the solution to the RD case was found, the SW parameters τ_u, τ_f, and d_0 were set in order to reproduce the same levels of stress at the onset and at the end of the breakdown process, as well as the same SW distance. Finally, the parameter R was tuned in order to have the same recurrence times, as described by equation (17) ($T_{\rm cycle} = 52.00$ yr for configuration A and $T_{\rm cycle} = 31.40$ yr for configuration B), for both the SW and RD models. The results, as predicted by the analytical solutions (4), (9), and (15) and their time derivatives, are plotted with thick lines in Figures 1 and 2 in the case of configuration A and in Figures 3 and 4 in the case of configuration B. In these figures, the numerical results pertaining to a system governed by the RD law, which are shown with thin lines, are also superimposed.

It can clearly be seen that the analytical solutions pertaining to model (1) were able to reproduce exactly the same $T_{\rm cycle}$ as the RD law (Figs. 1, 2a, 3, and 4a), as desired. This is not surprising, because the parameter R was set appropriately, as stated in the Subsequent Instabilities section. The

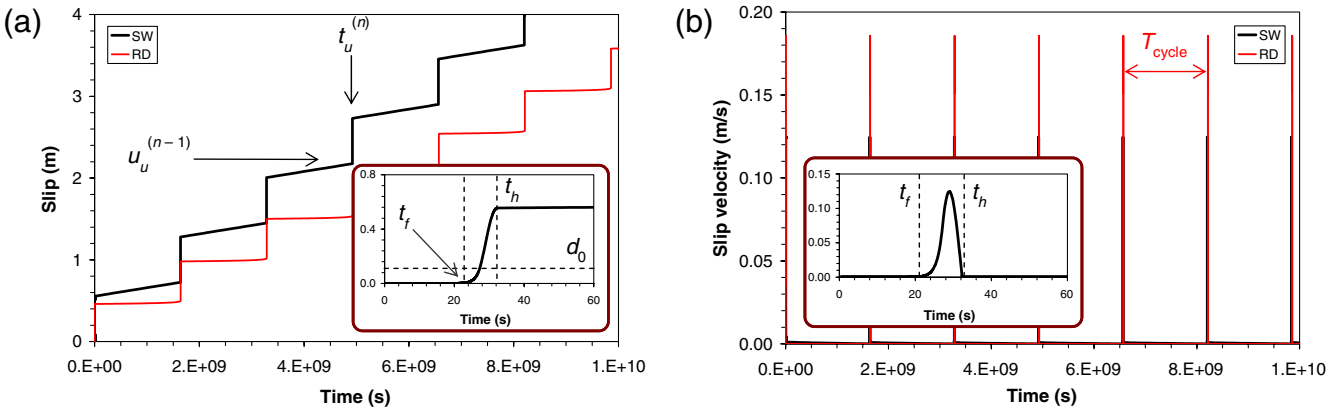

Figure 1. Evolution of the system as predicted by fully analytical solutions (thick lines; see the sections Fully Analytical Solution to the 1D Elastodynamic Equation and Subsequent Instabilities). The thin lines show a corresponding numerical solution pertaining to the RD model (equation 18). The parameter R of model (1) has been tuned to have the same interevent time as the RD case. Parts (a) and (b) show the time histories of the cumulative slip and slip velocity, respectively, with the inset showing the first instability event. The adopted parameters are those pertaining to configuration A listed in Table 1, which characterize a more unstable fault. The color version of this figure is available only in the electronic edition.

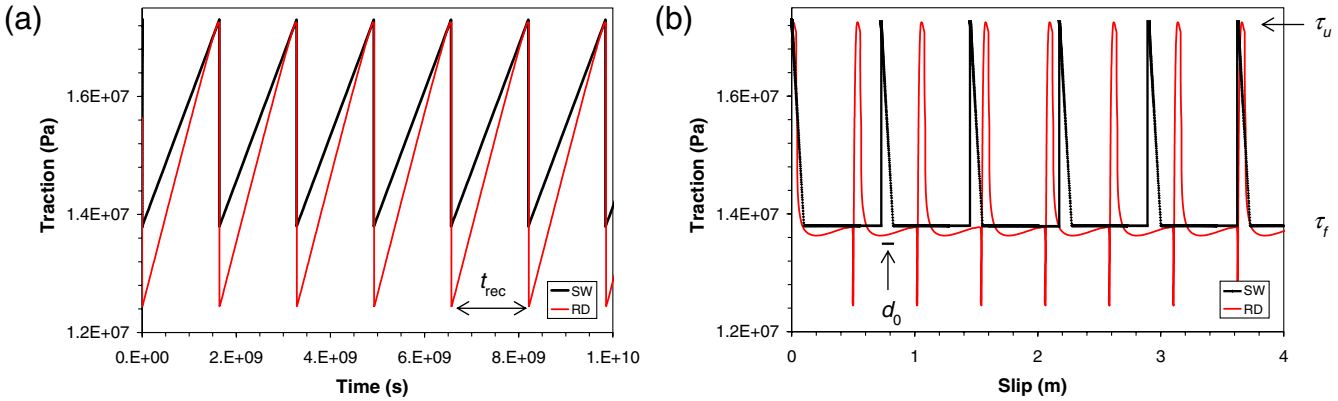

Figure 2. The same as in Figure 1, but now (a) reports the traction evolution as a function of time and (b) reports the traction versus slip. In (a), the recovery time (equation 11) for the SW case is also shown. The color version of this figure is available only in the electronic edition.

peaks in the velocity were lower in the SW case compared to the RD case, both for configuration A (Fig. 1b) and for configuration B (Fig. 3b). Similarly, the slip developed during each instability (i.e., the per-event slip $u^{(n)}$) was also smaller (Figs. 1a and 3a). On the contrary, the breakdown stress drop $\Delta\tau_b$ was identical for the two solutions, as expected (Figs. 2 and 4); note that the RD solution exhibits a dynamic overshoot after the release of stress that occurs during the accelerating phase of the rupture (Figs. 2b and 4b), which is not present in the SW solution. This overshoot was obtained also without the inclusion of the radiation damping term in the equation of motion (see Fig. A1d in the Appendix) and also for other types of RS laws (see fig. 1c in Bizzarri, 2010c). It was not predicted by the analytical solution because the SW law prescribes that, after the breakdown process, the frictional resistance equals τ_f and then increases accordingly to the recovery function f.

The dynamic overshoot in the RD law is associated with a more severe deceleration phase. While in the SW case $v = (1 - R)v_0$ in the whole interseismic stage (as discussed previously in the Interseismic Phase section), in the RD case the minimum of v is roughly one order of magnitude smaller. This difference is responsible for the different slips accumulated during the interseismic stage, or, in other words, for the different slopes of the envelope of the curves plotted in Figures 1a and 3a.

Discussion and Conclusions

In this study, two major goals were fulfilled. First, I derived a fully analytical solution to the 1D elastodynamic equation for a seismogenic fault (in particular, the one-body mass-spring analog fault system) governed by a linear, or classical, SW friction (Ida, 1972). Second, I proposed a suitable mechanism for the interseismic stress recovery to be incorporated in the linear SW framework, which makes it possible to simulate repeated instabilities on the same seismic structure. Note that this assumed interseismic traction history mimics the behavior of the RS friction laws, where the recurrence interval is not prescribed *a priori*, as in the present model, but it results as a numerical solution to the problem.

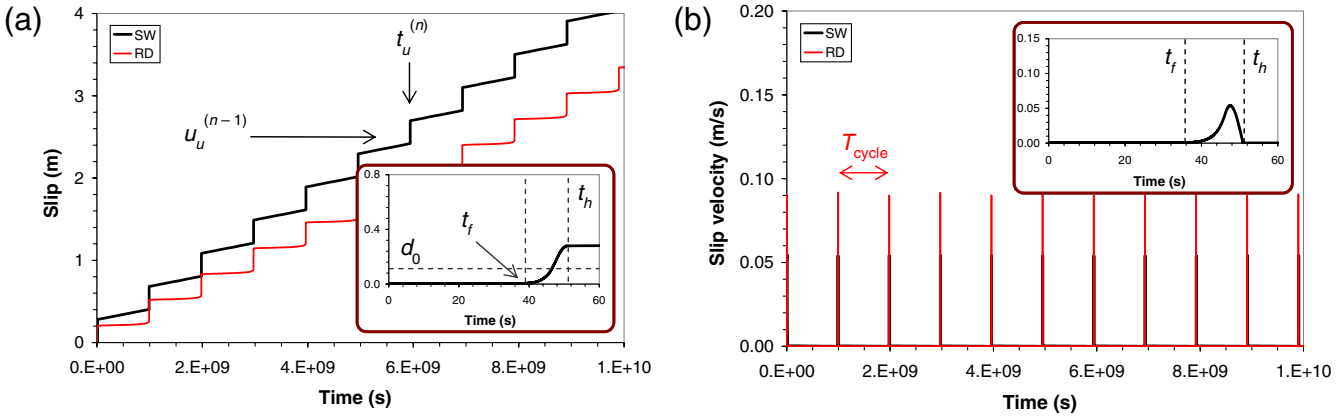

Figure 3. The same as in Figure 1 but now in the case for configuration B, which is representative of a fault with a moderate degree of instability. The color version of this figure is available only in the electronic edition.

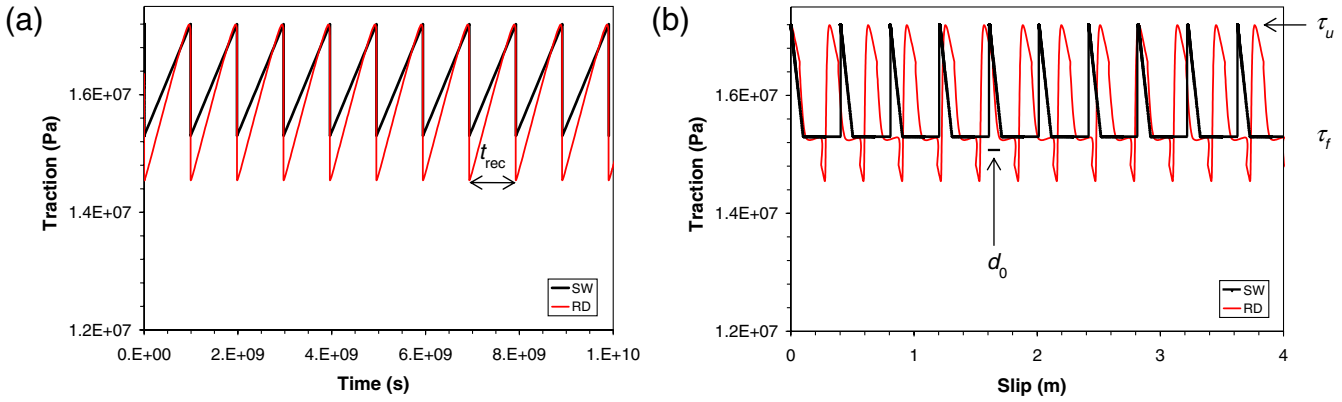

Figure 4. The same as in Figure 2 but now in the case for configuration B. The color version of this figure is available only in the electronic edition.

As a side result of the present study, it has been shown (see details in the Appendix) that the inclusion of the radiation damping term ($-c\dot{u}$) in the equation of motion (3) significantly affects the evolution of a system governed by the RD constitutive model. In particular, it causes a decrease in the peaks of the velocity attained during a slip instability (thus reducing the temperature developed by frictional heat), a decrease in the dynamic overshoot that occurs during the decelerating stage of the rupture, and therefore a reduction in the recurrence time. This confirms that the radiation damping does not merely affect the coseismic phase of a simulated earthquake event but also the whole history of the fault.

The analytical solutions presented in this paper (equations 4, 9, and 15 and their time derivatives) predict that the fault, after it undergoes a dynamic instability, develops a saturation slip and then heals (insets in Figs. 1a and 3a). Similarly, the slip velocity has a compact support (like a pulse; insets in Figs. 1b and 3b). This is corroborated by inferences from data (Heaton, 1990) and numerical experiments (Bizzarri, 2010a and references cited therein).

Overall, the behavior of the theoretical solution presented in this paper is compatible with a purely numerical solution to problem (3) in which an RS friction law (Ruina, 1983) was assumed, even if the per-event developed slip and the interseismic slip (and thus the total slip over multiple earthquake cycles) are different between the two models. Both of the constitutive models predict the same stress release during the coseismic slip, and this breakdown stress drop is constant in both models. Note that $\Delta\tau_b$ can potentially vary during the time evolution of the fault, and these variations already have been obtained in simulations when the thermal pressurization of pore fluids is associated with temporal changes in the slipping zone thickness, where the maximum deformation is concentrated (Bizzarri, 2010c). Moreover, both models show that the stress recovery occurs when the slip increases very slowly (see Figs. 2b and 4b), that is, when the sliding velocity is very low.

The possibility of simulating repeated instabilities within the SW framework can be regarded as an alternative to the widely used models that assume an RS constitutive law. The lively debate about the most appropriate governing law for the fault has been discussed elsewhere (e.g., Bizzarri, 2011b), and it is not the focus of the present paper.

The results indicate that the instability of the system is controlled by the dimensionless ratio

$$\kappa = \frac{\Delta\tau_b}{d_0 k}. \tag{19}$$

In particular, when $\kappa < 1$, an isolated fault system does not experience slip instabilities; on the contrary, as long as κ exceeds 1, the slider is more unstable in that the accumulated slip and the peaks in slip velocity are larger and the first instability occurs earlier. (Recall that the recurrence time is controlled by $\Delta\tau_b$; see equation 11.) This behavior is clearly visible from Figure 5 in which the solutions pertaining to different values of constitutive parameters (τ_u, τ_f, and d_0), leading to different values of the parameter κ, are plotted.

Within the framework of the RS laws, the more κ' exceeds 1, the more unstable the fault seems to be (e.g., Ruina, 1983; Gu *et al.*, 1984), where the dimensionless parameter κ' depends again on the constitutive parameters and on k:

$$\kappa' = \frac{k_{\rm cr}}{k} = \frac{(b-a)\sigma_n^{\rm eff}}{kL}. \tag{20}$$

The instability condition $\kappa > 1$ therefore suggests that the critical stiffness in the SW model is $k_{cr} = \Delta\tau_b/d_0$. Moreover, the condition $\kappa > 1$ for the SW law is the counterpart of the condition $\kappa' > 1$ already found for the RS laws. Notably, the condition $\kappa > 1$ is equivalent to $C_1 < 0$, which guarantees that the solutions (4) and (5) are real-valued functions (see the First Weakening Episode section).

Note that the analytical solution presented in this paper is based upon a governing model (the linear SW friction law)

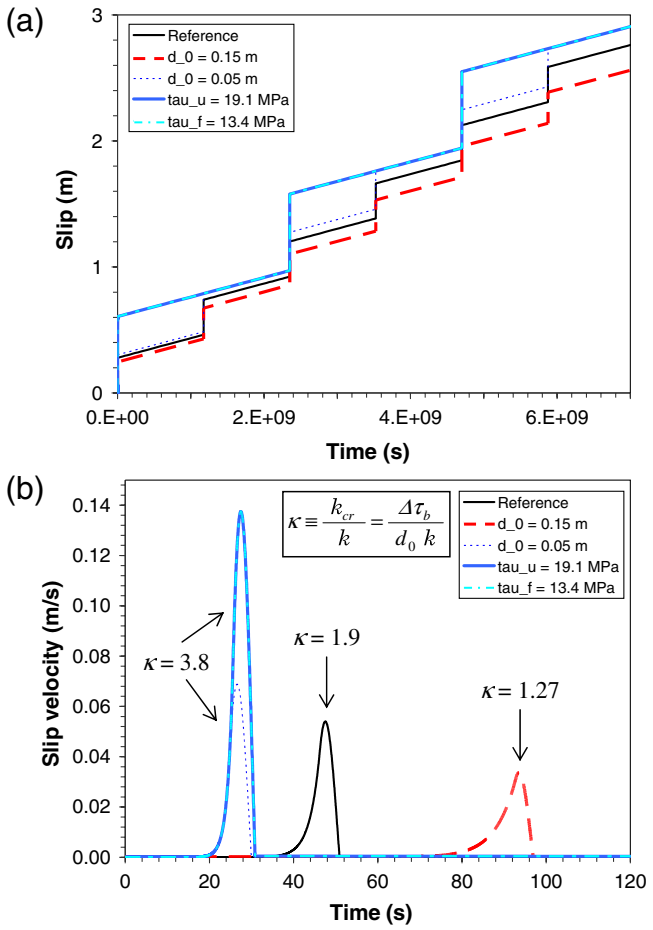

Figure 5. Effects of the model parameters (τ_u, τ_f, and d_0) on the evolution of the (a) slip and (b) slip velocity at the first instability. The thin continuous lines represent the same model as in Figures 3 and 4 (the reference parameters are those of configuration B in Table 1). The color version of this figure is available only in the electronic edition.

that provides a viable mechanism for the stress release with a finite energy flux at the crack tip. Therefore, it can be regarded as an extended version of the well-known exact solution to stick-slip events with an instantaneous transition for static to dynamic friction (e.g., Jaeger and Cook, 1976).

The present results assume that the fault maintains the same upper yield stress (τ_u) over its seismic cycle. In the SW framework, an instability occurs once the stress reaches the upper value τ_u (in some sense this defines a rupture criterion; incidentally, I report here that τ_u is also named yield strength), and therefore the fault has to recover the same amount of stress along its life. This assumption is confirmed by the behavior of a fault where an RS friction is assumed; in the case of the RD law (equation 18), the upper values of the frictional resistance (at which an instability occurs) are shown to always be the same, which is expected in the case of constant values of the governing parameters a, b, and σ_n^{eff} (see thin curves in Figs. 2 and 4), as I presently hypothesize.

I mention here that the hold-slide-hold laboratory experiments in the special case of stationary contacts (Dieterich, 1972; Teufel and Logan, 1978) have revealed that the coefficient of static friction μ_s (which corresponds to the quantity μ_u) increases with the logarithm of time:

$$\mu_s = \mu_* + K \log\left(\frac{t - t_f}{t_*} + 1\right), \tag{21}$$

where K is an empirical dimensionless constant retrieved from fitting procedures, t_f is the time occurrence of the last instability (see also the Fully Analytical Solution to the 1D Elastodynamic Equation section), and the normalizing constant $t_* = 1$ s is used for dimensional correctness. (Consequently, $t - t_f$ represents the duration of the contact between the two sliding surfaces, that is, the hold time; see also Marone, 1998 and references cited therein.) The increase in μ_s predicted by equation (21) leads to the so-called logarithmic healing that occurs in the interseismic period; note that the healing of slip at the end of the slip pulse observed in the framework of my model is a different phenomenon. In addition, note that an open question remains as to whether the above-mentioned results (obtained for slow slip rates, $< 10^{-3}$ m/s) can be applied to natural faults moving at $v \sim 1 - 10$ m/s or more.

In the present paper, I made the assumption that the stress recovery is linear with time, as stated by equation (2). Interestingly, in the case of the RD law, where the stress recovery is not imposed but is completely controlled by the nonlinear governing equations, the stress recovery is shown to be linear over the whole life of the fault (see Figs. 2a and 4a).

Finally, I highlight that, in the coseismic time window, the solution for the slip velocity (equations 5 and 10) presented here is not based on special physical assumptions (like the solution in the interseismic phase, which depends on the stress recovery mechanism that was assumed). Equations (5) and (10) are nonsingular, dynamically consistent by definition, and agree with previously assumed functions (e.g., Liu and Archuleta, 2004). As such, they can be regarded as possible candidates for a source time function to be employed in kinematic slip inversions of strong-motion data. The solution derived here exhibits a rapid decrease after its peaks, and this could cause significant radiation of seismic waves also at the healing front; this will be examined in a future study devoted to the finite source inversion problem.

Data and Resources

All data sources were taken from published works listed in the References.

Acknowledgments

J.-H. Wang and P. Spudich are kindly acknowledged for stimulating discussions. I also thank Associate Editor D. D. Oglesby and two anonymous referees, who provided stimulating comments that greatly improved the manuscript.

References

Aochi, H., and M. Matsu'ura (2002). Slip- and time-dependent fault constitutive law and its significance in earthquake generation cycles, *Pure Appl. Geophys.* **159,** no. 9, 2029–2044, doi 10.1007/s00024-002-8721-z.

Bizzarri, A. (2009). What does control earthquake ruptures and dynamic faulting? A review of different competing mechanisms, *Pure Appl. Geophys.* **166,** no. 5–7, 741–776, doi 10.1007/s00024-009-0494-1.

Bizzarri, A. (2010a). Pulse-like dynamic earthquake rupture propagation under rate-, state- and temperature-dependent friction, *Geophys. Res. Lett.* **37,** L18307, doi 10.1029/2010GL044541.

Bizzarri, A. (2010b). On the relations between fracture energy and physical observables in dynamic earthquake models, *J. Geophys. Res.* **115,** no. B10307, doi 10.1029/2009JB007027.

Bizzarri, A. (2010c). On the recurrence of earthquakes: Role of wear in brittle faulting, *Geophys. Res. Lett.* **37,** L20315, doi 10.1029/2010GL045480.

Bizzarri, A. (2011a). Temperature variations of constitutive parameters can significantly affect the fault dynamics, *Earth Planet. Sci. Lett.* **306,** 272–278, doi 10.1016/j.epsl.2011.04.009.

Bizzarri, A. (2011b). On the deterministic description of earthquakes, *Rev. Geophys.* **49,** RG3002, doi 10.1029/2011RG000356.

Bizzarri, A. (2012). Effects of permeability and porosity evolution on simulated earthquakes, *J. Struct. Geol.*, doi 10.1016/j.jsg.2011.07.009 (in press).

Bizzarri, A., and M. Cocco (2006). A thermal pressurization model for the spontaneous dynamic rupture propagation on a three-dimensional fault: 1. Methodological approach, *J. Geophys. Res.* **111,** no. B05303, doi 10.1029/2005JB003862.

Bizzarri, A., M. Cocco, D. J. Andrews, and E. Boschi (2001). Solving the dynamic rupture problem with different numerical approaches and constitutive laws, *Geophys. J. Int.* **144,** 656–678.

Cocco, M., and A. Bizzarri (2002). On the slip-weakening behavior of rate- and state dependent constitutive laws, *Geophys. Res. Lett.* **29,** no. 11, doi 10.1029/2001GL013999.

Dieterich, J. H. (1972). Time-dependent friction in rocks, *J. Geophys. Res.* **77,** 3690–3697.

Gu, J. C., J. R. Rice, A. L. Ruina, and S. T. Tse (1984). Slip motion and stability of a single degree of freedom elastic system with rate and state dependent friction, *J. Mech. Phys. Solid.* **32,** 167–196.

Heaton, T. H. (1990). Evidence for and implications of self-healing pulses of slip in earthquake rupture, *Phys. Earth Planet. In.* **64,** 1–20, doi 10.1016/0031-9201(90)90002-F.

Ida, Y. (1972). Cohesive force across the tip of a longitudinal-shear crack and Griffith's specific surface energy, *J. Geophys. Res.* **77,** no. 20, 3796–3805.

Jaeger, J., and N. G. Cook (1976). *Fundamentals of Rock Mechanics*, Chapman and Hall, London, 585 pp.

Lapusta, N., and Y. Liu (2009). Three-dimensional boundary integral modeling of spontaneous earthquake sequences and aseismic slip, *J. Geophys. Res.* **114,** no. B09303, doi 10.1029/2008JB005934.

Liu, P., and R. J. Archuleta (2004). A new nonlinear finite fault inversion with three-dimensional Green's functions: Application to the 1989 Loma Prieta, California, earthquake, *J. Geophys. Res.* **109,** no. B02318, doi 10.1029/2003JB002625.

Marone, C. (1998). Laboratory-derived friction laws and their application to seismic faulting, *Annu. Rev. Earth Planet. Sci.* **26,** 643–696.

Mitsui, Y., and M. Cocco (2010). The role of porosity evolution and fluid flow in frictional instabilities: A parametric study using a spring-slider dynamic system, *Geophys. Res. Lett.* **37,** L233305, doi 10.1029/2010GL045672.

Mitsui, Y., and K. Hirahara (2009). Coseismic thermal pressurization can notably prolong earthquake recurrence intervals on weak rate and state friction faults: Numerical experiments using different constitutive equations, *J. Geophys. Res.* **114,** no. B09304, doi 10.1029/2008JB006220.

Okubo, P. G. (1989). Dynamic rupture modeling with laboratory-derived constitutive relations, *J. Geophys. Res.* **94,** no. B9, 12,321–12,335.

Rice, J. R. (1993). Spatio-temporal complexity of slip on a fault, *J. Geophys. Res.* **98,** 9885–9907, doi 10.1029/93JB00191.

Rice, J. R., and S. T. Tse (1986). Dynamic motion of a single degree of freedom system following a rate and state dependent friction, *J. Geophys. Res.* **91,** no. B1, 521–530.

Ruina, A. L. (1983). Slip instability and state variable friction laws, *J. Geophys. Res.* **88,** no. B12, 10,359–10,370.

Scholz, C. H. (1988). The critical slip distance for seismic faulting, *Nature* **336,** 761–763.

Teufel, L. W., and J. M. Logan (1978). Effect of displacement rate of the real area of contact and temperatures generated during frictional sliding of Tennessee sandstone, *Pure Appl. Geophys.* **116,** 840–872.

Walsh, J. B. (1971). Stiffness in faulting and in friction experiments, *J. Geophys. Res.* **76,** no. 35, 8597–8598.

Appendix

Numerical Solution to the 1D Dynamic Problem in the Case of the RD Model

When the spring-slider dashpot model is coupled with rate- and state-friction law (18), the dynamic problem has to be solved numerically. This is done using a code implementing a fourth-order Runge–Kutta method with adaptive time stepping and a control of the truncation error. The methodology is exactly the same as in previous papers (e.g., Bizzarri, 2010c), where the following equation of motion was considered:

$$m\ddot{u} = kv_{\text{load}}t - ku - \tau. \tag{A1}$$

In the present paper, equation (3) was considered, rewritten here for completeness:

$$m\ddot{u} = kv_{\text{load}}t - ku - \tau - c\dot{u}, \tag{A2}$$

which is identical to equation (A1) except for the presence of the radiation damping term ($-c\dot{u}$), henceforth referred to as RDT. As mentioned in the Fully Analytical Solution to the 1D Elastodynamic Equation section, this term mimics the energy loss as propagating seismic waves, which are fully considered in extended fault models (e.g., 2D or 3D fault models) and neglected by definition in the single spring-slider approximation of a fault (1D fault model).

In the present section, the effects of the introduction of such a term in the solutions obtained by assuming the RD law (equation 18) are quantitatively evaluated. I focus on configuration B of Table 1; the results are qualitatively the same for other values of the governing parameters.

The results reported in Figure A1 show that the presence of the RDT reduces the peaks in the slip velocity history by about a factor of 2 (from 0.36 to 0.18 m/s; see Fig. A1b). These differences cause the configuration without the RDT to develop large values of per-event slip, as shown in Figure A1a. Interestingly, the presence of the RDT does not

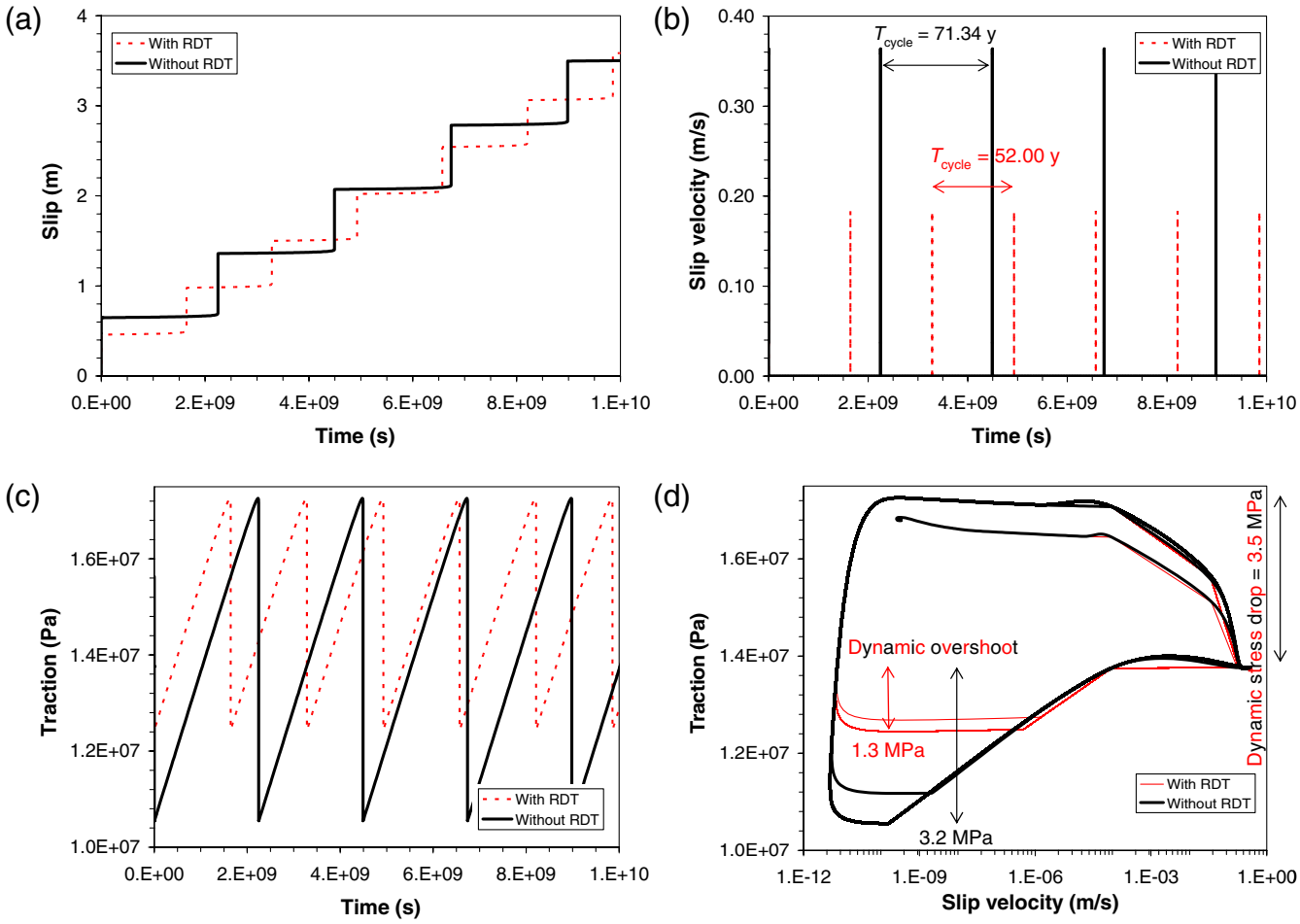

Figure A1. Comparison between numerical solutions in the case of the RD law (equation 18) with and without the RDT (dashed and continuous curves, respectively). (a) Time history of the slip, (b) time history of the slip velocity, (c) time history of the frictional resistance, and (d) phase portrait (i.e., traction versus slip velocity). Parameters are those of configuration A in Table 1. The color version of this figure is available only in the electronic edition.

change the upper value attained by the frictional resistance (see Fig. A1c). On the contrary, it also causes a significant difference in the breakdown process; from Figure A1d, note that while the dynamic stress drop (occurring within the accelerating phase of the rupture) is the same in both cases (it equals 3.5 MPa), the dynamic overshoot (taking place during the decelerating stage of the rupture) is rather different. Without the RDT, the fault exhibits a dynamic overshoot of 3.2 MPa; while with the RDT, it has a dynamic overshoot of 1.3 MPa. This difference explains the different recurrence time (T_{cycle}) of the two configurations; without the RDT, the fault takes more time to reach again a new instability, because it has to recover more stress with respect to the case where the RDT is considered. This is clearly visible from Figure A1b, from which T_{cycle} for the case with the RDT is about 34% shorter than that predicted in the case without the RDT.

Istituto Nazionale di Geofisica e Vulcanologia
Sezione di Bologna
Via Donato Creti 12
40128 Bologna BO
Italy
bizzarri@bo.ingv.it

Manuscript received 10 May 2011